MOLECULAR AND CELLULAR BIOLOGY, Feb. 2008, p. 1285–1297 Vol. 28, No. 4
0270-7306/08/$08.00+0 doi:10.1128/MCB.01332-07

Abnormal Heart Development and Lung Remodeling in Mice Lacking the Hypoxia-Inducible Factor-Related Basic Helix-Loop-Helix PAS Protein NEPAS▽

Toshiharu Yamashita,[1]† Osamu Ohneda,[1]†* Masumi Nagano,[1] Motoyuki Iemitsu,[2] Yuichi Makino,[5] Hirotoshi Tanaka,[5] Takashi Miyauchi,[3] Katsutoshi Goto,[4] Kinuko Ohneda,[6] Yoshiaki Fujii-Kuriyama,[7] Lorenz Poellinger,[8] and Masayuki Yamamoto[9]*

Department of Regenerative Medicine[1] and Department of Molecular Pharmacology,[4] Institute of Basic Medical Sciences, Institute of Health and Sport Sciences,[2] and Cardiovascular Division of Department of Internal Medicine, Institute of Clinical Medicine,[3] University of Tsukuba, 1-1-1 Tennoudai, Tsukuba 305-8575, Japan; Division of Clinical Immunology, The University of Tokyo, 4-6-1 Shirokanedai, Minato-ku, Tokyo 108-8639, Japan[5]; Laboratory of Molecular Pathophysiology, Faculty of Pharmacy, Takasaki University of Health and Welfare, 60 Nakaorui-machi, Takasaki 370-0033, Japan[6]; Center for TARA and JST-SORST project, University of Tsukuba, 1-1-1 Tennoudai, Tsukuba 305-8577, Japan[7]; Department of Cell and Molecular Biology, Medical Nobel Institute, Karolinska Institute, S-171 77 Stockholm, Sweden[8]; and Center for TARA and JST-ERATO Environmental Response Project, 1-1-1 Tennoudai, Tsukuba 305-8577, and Tohoku University Graduate School of Medicine, 2-1 Seiryo-cho, Aoba-ku, Sendai 980-8575, Japan[9]

Received 25 July 2007/Returned for modification 8 September 2007/Accepted 20 November 2007

Hypoxia-inducible factors (HIFs) are crucial for oxygen homeostasis during both embryonic development and postnatal life. Here we show that a novel HIF family basic helix-loop-helix (bHLH) PAS (Per-Arnt-Sim) protein, which is expressed predominantly during embryonic and neonatal stages and thereby designated NEPAS (neonatal and embryonic PAS), acts as a negative regulator of HIF-mediated gene expression. NEPAS mRNA is derived from the *HIF-3α* gene by alternative splicing, replacing the first exon of HIF-3α with that of inhibitory PAS. NEPAS can dimerize with Arnt and exhibits only low levels of transcriptional activity, similar to that of HIF-3α. NEPAS suppressed reporter gene expression driven by HIF-1α and HIF-2α. By generating mice with a targeted disruption of the *NEPAS*/*HIF-3α* locus, we found that homozygous mutant mice (*NEPAS*/*HIF-3α*$^{-/-}$) were viable but displayed enlargement of the right ventricle and impaired lung remodeling. The expression of endothelin 1 and platelet-derived growth factor β was increased in the lung endothelial cells of NEPAS/HIF-3α-null mice. These results demonstrate a novel regulatory mechanism in which the activities of HIF-1α and HIF-2α are negatively regulated by NEPAS in endothelial cells, which is pertinent to lung and heart development during the embryonic and neonatal stages.

Hypoxia-inducible factors (HIFs) are crucial for oxygen homeostasis during both embryonic development and postnatal life. HIFs are heterodimeric transcription factors consisting of α and β subunits. To date, three α subunits (HIF-1α, HIF-2α, and HIF-3α) and one β subunit (HIF-1β, also called Arnt [aryl hydrocarbon receptor nuclear translocator]) have been identified (10, 34, 37). Oxygen-dependent activity of HIFs is mainly regulated through the stability of their α subunits. Under the normoxic condition, HIF-α protein is rapidly degraded through the ubiquitin-proteasomal pathway. During this process, HIF-α is hydroxylated by proline hydroxylases and specifically interacts with the von Hippel-Lindau (VHL) tumor suppressor protein (8, 21), which acts as a component of E3 ubiquitin ligase and targets HIF-α molecules for ubiquitination and subsequent degradation (12). Under low oxygen tension, hydroxylation of HIF-α is significantly reduced because the activity of proline hydroxylases is repressed by hypoxia. Since VHL can recognize exclusively the hydroxylated HIF-α molecules, in the hypoxic condition HIF-α is stabilized and activates transcription of target genes with Arnt in the nucleus.

Although it is indisputable that this ubiquitin-proteasomal pathway plays a central role in determining HIF activity, an additional regulatory mechanism should be considered under certain conditions. For instance, the availability of oxygen is limited in utero and embryos are continuously exposed to hypoxia (17). Under such conditions, it is likely that HIF-α proteins are no longer degraded and accumulate into the nucleus. Given the fact that both HIF-1α and HIF-2α are required for early embryonic development (13, 25, 33), HIF activity must be elaborately regulated in the embryos.

To elucidate the regulatory mechanisms of HIF activity during the embryonic stage, in this study we focused on the products of the *HIF-3α* gene, the third member of the HIF-α family. HIF-3α retains a basic helix-loop-helix (bHLH) and PAS (Per-Arnt-Sim) domain that shows high similarity with those of HIF-1α and HIF-2α. Utilizing the bHLH PAS do-

* Corresponding author. Mailing address for Osamu Ohneda: Department of Regenerative Medicine, Institute of Basic Medical Sciences, University of Tsukuba, 1-1-1 Tennoudai, Tsukuba 305-8575, Japan. Phone and fax: 81-29-853-2938. E-mail: oohneda@md.tsukuba.ac.jp. Mailing address for Masayuki Yamamoto: Tohoku University Graduate School of Medicine, 2-1 Seiryo-cho, Aoba-ku, Sendai 980-8575, Japan. Phone: 81-22-717-8084. Fax: 81-22-717-8090. E-mail: masi@mail.tains.tohoku.ac.jp.

† T. Yamashita and O. Ohneda contributed equally to this work.

▽ Published ahead of print on 10 December 2007.

main, HIF-3α can dimerize with Arnt, and the resulting heterodimer (i.e., HIF-3α–Arnt) binds to the hypoxia-responsive element (HRE). In contrast, HIF-3α lacks the C-terminal transactivation domain (CTAD [10]). Therefore, whereas HIF-3α retains another transactivation domain, the N-terminal transactivation domain (NTAD), its transcriptional activity is much weaker than that of HIF-1α and HIF-2α (11). It has been reported that HIF-3α acts as a competitor against HIF-1α or HIF-2α by recruiting a common partner, Arnt, and occupying the HRE sequences (11).

A splicing variant product of the *HIF-3*α gene, IPAS (inhibitory PAS protein), is known to act as an inhibitor of transcription, because IPAS lacks both the NTAD and the CTAD. IPAS possesses a first exon (exon 1a) distinct from that of HIF-3α (exon 1b [18, 19]). The expression of IPAS is induced by hypoxia, while that of HIF-3α is independent of hypoxia. This may be due to the presence of functional HREs upstream of exon 1a, while no such HRE resides in the regulatory region of exon 1b. An intriguing observation in this regard is that HIF-3α mRNA is downregulated but IPAS mRNA is induced by hypoxia in mouse heart and lung (18), suggesting that the induction of IPAS by hypoxia acts as a potential negative feedback system in the regulation of HIF target gene expression.

In this study we found a novel hypoxia-inducible product of the *HIF-3*α gene. This product is a splicing variant of the *HIF-3*α gene and referred to as NEPAS (neonatal and embryonic PAS protein). NEPAS is expressed almost exclusively in the late embryonic and early postnatal stages, and the expression is predominant in the lung and heart. This is in contrast to the expression profile of HIF-3α, as HIF-3α mRNA is rarely detectable during embryonic and neonatal stages. Targeting disruption of the *HIF-3*α gene in mice revealed that without NEPAS the lung remodeling is severely impaired, resulting in hypertrophy of the right ventricle (RV) and pulmonary hyperplasia. Furthermore, we found that the expression of endothelin 1 (ET-1) is upregulated in the mutant lung, suggesting that negative regulation of ET-1 expression by NEPAS is important for lung development. These results thus demonstrate that NEPAS acts as a regulator that represses HIF activity during embryonic and neonatal development.

MATERIALS AND METHODS

RNA preparation and RT-PCR. Total RNAs were prepared from various tissues and cells, and cDNAs were synthesized from total RNAs (1 μg) using a reverse transcription-PCR (RT-PCR) kit (Clontech, Mountain View, CA). Aliquots (1 μl) of the cDNA solution were amplified using PCR. The PCR procedure consisted of appropriate cycles of 95°C for 30 s and 68°C for 1 min. The PCR products were electrophoretically separated on 2% agarose gels. The primers used for the PCRs were as follows: primer a, 5′-GAGGGTTTCGTCATGG TAC-3′; primers b and d, 5′-TCTTGAAGTTCCTCTTGGTC-3′; primer c, 5′-ATGGCGTTGGGGCTGCACGCGTG-3′; ET-1 5′ primer, 5′-CACCGGAGC TGAGAATGGAGTGCAG-3′; ET-1 3′ primer, 5′-CGCACTGACATCTAAC TGCCTGGTC-3′; $VEGF_{164}$ 5′ primer, 5′-CTTTACTGCTGTACCTTCACCA TGC-3′; $VEGF_{164}$ 3′ primer, 5′-AACAAGGCTCACAAGTGATTTTCTGG-3′; 18S rRNA 5′ primer, 5′-TATCAGATCAAAACCAACCCGGTGAGC-3′; 18S rRNA 3′ primer, 5′-CCAATTACAGGGCCTCGAAAGAGTCCT-3′; Arnt 5′ primer, 5′-CAGGTGCCCACCCAGGCTACAGCCA-3′; Arnt 3′ primer, 5′-GGCTAGGTGCTTGTGCTTGTGTCTG-3′; HIF-1α 5′ primer, 5′-CAAGAT CTCGGCGAACGAAAGAGTCTGA-3′; HIF-1α 3′ primer, 5′-GAAGCACCT TCCACGTTGCTGACTTGAT-3′; HIF-2 α 5′ primer, 5′-CAGCTCAGAGCT GAGGAAGG-3′; HIF-2α 3′ primer, 5′-GTTGTAGACTCTCACTTGCC-3′; Flk-1 5′ primer, 5′-AGGACCAAGGCGACTATGTTTGCTCTG-3′; Flk-1 3′ primer, 5′-ACGGTCCGTACGAGAATGACAAGAAGG-3′; platelet-derived growth factor β (PDGF-β) 5′ primer, 5′-TCCGGAGTCGAGTTGGAAAG CTCATCT-3′; PDGF-β 3′ primer, 5′-GGGTGTGCTTAAACTTTCGGTGC TTGC-3′.

Cloning of NEPAS. A NEPAS full-length cDNA clone was isolated from an E16.5 lambda phage cDNA library (Becton Dickinson, Franklin Lakes, NJ). Screening probes were from the second exon sequence of *HIF-3*α, and library screening was performed using a nonradioisotope labeling kit and detection reagents (Amersham Biosciences, Buckinghamshire, England). The phages were digested with protease K (Wako, Osaka, Japan) and isolated for positive cDNA clones. After the purification, a NEPAS fragment was subcloned into NotI-digested pBluescript SK(+) plasmid (Stratagene, La Jolla, CA) and sequenced using a DNA sequencer (Applied Biosystems 310A; Foster City, CA).

Construction of a *NEPAS*/*HIF-3*α-targeting vector and generation of *NEPAS*/*HIF-3*α-null mice. A genomic DNA sequence containing the second exon of *NEPAS*/*HIF-3*α was cloned from a 129/SV mouse bacterial artificial chromosome clone. A targeting vector was constructed by replacing part of the second exon and the following intron of the *NEPAS*/*HIF-3*α gene with a neomycin resistance (Neo^r) gene sandwiched between *loxP* sequences and the green fluorescent protein (GFP) gene (*GFP*), with a diphtheria toxin gene placed at the 3′ end as a positive selection marker. This chimeric DNA was then cloned into pBluescript SK(+). The linearized vector was electroporated into E14 embryonic stem (ES) cells derived from 129/SV mice. After electroporation, cells were cultured with G418 (300 μg/ml; Invitrogen, San Diego, CA) for negative selection to isolate neomycin-resistant clones. DNA from the isolated clones was screened by PCR for homologous recombination and subsequently confirmed by Southern blot analysis. Following proliferation, recombinant ES cells were injected into C57BL/6J blastocysts and surgically implanted into the uterus of pseudopregnant ICR foster mothers. Chimeric mice were then intercrossed with C57BL/6J mice, and offspring were genotyped.

Immunohistochemistry and section staining. Isolated tissues were fixed in 4% paraformaldehyde/phosphate-buffered saline (PBS) overnight, washed three times with PBS, and embedded in polyester wax. Sections (5 μm) were cut for immunohistochemical and hematoxylin-eosin staining. These sections were immunohistochemically stained with anti-CD31 (PharMingen, San Diego, CA), antidesmin (DAKO, Glostrup, Denmark), anti-surfactant-associated protein D (anti-SP-D) (Santa Cruz, CA) (4), and anti-HIF-2α or anti-HIF-1α and anti-GFP (Becton Dickinson) antibodies overnight at 4°C as previously described (23). After being washed with PBS containing 0.1% Tween 20, the slides were further incubated with horseradish peroxidase-conjugated goat anti-rabbit immunoglobulin G (IgG) antibody (Biosource, San Diego, CA). Positive signals were visualized with 3,3′-diaminobenzidine with or without $NiCl_2$. Counterstaining was carried out using nuclear fast red or hematoxylin. Victoria blue-van Gieson staining was performed using Victoria blue reagent and a van Gieson reagent kit (Muto, Tokyo, Japan). To assess the frequency of microvessels in the lung (less than 30 μm in diameter, except for capillaries), we counted the number of vessels surrounded by elastin fibers by microscopy. We counted more than 100 vessels per mouse ($n = 5$) and evaluated the frequency of each type of vessel.

Measurement of RV pressure and heart echo analysis. On the day of the experiment, mice were anesthetized with sodium pentobarbital. Transthoracic echocardiography was performed with an ultrasound biomicroscopy-echocardiographic system (Vevo 660; Visual Sonics, Ontario, Canada) equipped with a 25-MHz scanning probe. To obtain a two-dimensional short-axis view (B-mode images) of the left ventricle (LV) and RV, the papillary muscles of the LV were used as a landmark. Left and right ventricular end-diastolic dimensions (mm^2) were measured using Vevo analytical software (VS-MMD; Visual Sonics). After the echocardiographic measurement, a 26-gauge needle was connected to a silastic catheter and placed into the right ventricular cavity by direct puncture of the RV. Right ventricular systolic pressure was measured using a pressure transducer (SCK-590; Gould) and a computerized data acquisition system (MP100A-CA; Biopac, Santa Barbara, CA) at a sampling rate of 1,000 Hz. The body temperature of the mice was maintained at 37°C using small-animal warmers. Their heart rates under these conditions were between 300 and 500 beats per minute.

Cell culture and transfection experiments. Lungs were dissected from wild-type and *NEPAS*/*HIF-3*$\alpha^{-/-}$ mice at postnatal day 15 (P15). Lung cell suspensions were prepared by collagenase digestion and stained with allophycocyanin-conjugated anti-CD31 antibody (PharMingen). Lung vascular endothelial cells were purified using FACSVantage (Becton Dickinson). Subsequently, these cells were cultured in HAVA medium (24) in the presence of endothelial cell growth supplement (Becton Dickinson) on collagen type I-coated dishes (Becton Dickinson). After reaching 50% confluence, cells were infected with polyoma middle-T-antigen retrovirus/Neo^r as described previously (24). Cells were maintained in

HAVA medium without the addition of any growth supplement. Lung endothelial cells were then transfected with pBOS-NEPAS, pBOS-Arnt, pBOS-HIF-1α, or pBOS-HIF-2α using FuGENE 6 transfection reagent (Roche, Indianapolis, IN). After a 2-day incubation, 100 μM $CoCl_2$ was added to the dish. Cells were harvested with a rubber scraper after 12 h, and total RNA was isolated for RT-PCR analysis.

GAL4 two-hybrid assay and HRE-Luc reporter assay. We transfected a reporter gene plasmid (1 ng), pGAL-DBD-Arnt (10 ng), pGAL-VP16AD-NEPAS (5 or 25 ng), or pGAL-VP16AD-HIF-3α (5 or 25 ng) into 293T cells using FuGENE 6 (Roche). A reporter assay was also performed by cotransfecting HREx4-Luc (10 ng), pBOS-HIF-1α (10 ng), pBOS-HIF-2α (10 ng), pBOS-HIF-3α (10 ng), pBOS-NEPAS (10 ng), or pBOS-Arnt (10 ng) into 293T cells. The pEF-Renilla-Luc plasmid (1 ng) was cotransfected as a control in both reporter assays. Cells were exposed to $CoCl_2$ (100 μM) for 12 h before harvest.

Western blot analysis. Nuclear extracts (50 μg) prepared from endothelial cells were electrophoresed on a 10% sodium dodecyl sulfate (SDS)-polyacrylamide gel and transferred onto a polyvinylidene difluoride membrane (Millipore, Billerica, MA). Blocking was performed at room temperature for 1 h in Tris-buffered saline (TBS) with 5% nonfat milk. The membranes were incubated with rabbit anti-HIF-2α antibody (6) or anti-HIF-1α antibody (Novus Biologicals, Littleton, CO) in TBS containing 5% nonfat milk. After being washed with TBS containing 0.1% Tween 20, the membrane was incubated with horseradish peroxidase-conjugated goat anti-rabbit IgG (Zymed, San Francisco, CA) or goat anti-mouse IgG (Zymed) in TBS with 5% nonfat milk. Subsequently, proteins were detected by enhanced chemiluminescence (Amersham Biosciences). Goat anti-lamin B antibody (Santa Cruz) was used to monitor protein loading and transfer.

Analysis of ET-1 expression. *NEPAS*/*HIF-3*$\alpha^{-/-}$ and wild-type lung endothelial cells were treated under normoxic conditions or in the presence of $CoCl_2$. Harvested cytosol extracts were analyzed with an enzyme-linked immunosorbent assay (ELISA) kit for ET-1 (R&D Systems, Minneapolis, MN). Total protein concentration of cytosol extracts was measured with the Bio-Rad protein assay (Bio-Rad Laboratories, Hercules, CA). ET-1 protein expression was measured according to the manufacturer's instructions (R&D Systems).

Chromatin immunoprecipitation (ChIP) assay. For each assay, 5×10^6 wild-type and *NEPAS*/*HIF-3*$\alpha^{-/-}$ lung endothelial cells were fixed with 1% formaldehyde for 10 min at room temperature, washed with PBS containing 1 μM protease inhibitor cocktail (PIC) (Roche), harvested, and treated with hypotonic solution (5 mM HEPES, 85 mM KCl, 0.5% NP-40, and 1 μM PIC). Nuclei were collected after centrifugation at 14,000 × *g* for 5 min and then lysed with lysis buffer (50 mM Tris-HCl [pH 8.1], 10 mM EDTA, 1% SDS, and 1 μM PIC). After fragmentation of DNA by sonication, immunoprecipitation reactions were performed using a rotating mixer at 4°C with 1 μg/ml anti-HIF-1α antibody (Novus Biologicals) or anti-HIF-2α antibody (23). Normal mouse IgG or rabbit IgG was employed as a negative control to verify the specificity of the reaction. Following incubation with the antibody, reaction mixtures were incubated with preblocked protein A-agarose beads (Calbiochem, La Jolla, CA) at 4°C for 1 h and precipitated complexes were collected by centrifugation at 3,000 × *g* for 5 min. These complexes were washed three times with wash buffer (0.25 mM LiCl, 1% NP-40, 1% sodium deoxycholate, 1 mM EDTA, and 10 mM Tris-HCl [pH 8.1]) and eluted from the protein A-agarose beads with elution buffer (1% SDS and 0.1 M $NaHCO_3$). DNA-protein complexes were separated from the agarose beads by centrifugation at 4°C at 3,000 × *g* and denatured at 65°C for 4 h. DNA fragments were then extracted with phenol-chloroform, precipitated with ethanol, and resuspended in TE buffer (10 mM Tris-HCl [pH 7.5] and 1 mM EDTA) for detection of ET-1 HRE sequence by PCR using *Taq* DNA polymerase (Sigma-Aldrich, St. Louis, MO). The following primers were used for the PCR analysis: forward, 5′-TGGATTGTCAGACGGCGGGCGTCTGC-3′, and reverse, 5′-CAGACCGGGTCAGGCTCTCAGCGCCG-3′.

Nucleotide sequence accession number. The cDNA sequence of NEPAS was registered with GenBank, and its accession number is AB289606.

RESULTS

A novel splicing variant of HIF-3α. While investigating the functional roles of the HIF-3α gene splicing variant IPAS (18, 19) in regulating the activities of HIF-1α and HIF-2α, we discovered a new HIF-3α splicing variant, NEPAS. In RT-PCR experiments designed to investigate IPAS mRNA expression in mouse embryos, two primer sets (primer sets a-b and c-d in Fig. 1A, top) did not detect the expected IPAS band but detected a product of unexpectedly smaller size in fetal and neonatal mice from embryonic day 15.5 (E15.5) to P15 (Fig. 1A, bottom). A full-length NEPAS cDNA was isolated from an E16.5 whole-embryo cDNA library, and the analysis of the cDNA revealed that NEPAS mRNA contains a novel open reading frame of 1,992 nucleotides encoding a polypeptide of 664 amino acids (Fig. 1B). The first eight amino acids are encoded by the IPAS-specific first exon (exon 1a), followed by the 2nd to 15th exons of the HIF-3α gene. Thus, it represents a novel splicing variant of HIF-3α (Fig. 1C, left), in which the first exon is replaced with the IPAS first exon, indicating that the predicted polypeptide retains an NTAD but lacks the robust transcriptional activation function of the CTAD (Fig. 1C, right panel) (10, 22).

Transcriptional activity of NEPAS. We performed Gal4 two-hybrid assays to determine the potential partner proteins of NEPAS and found that, like HIF-3α, NEPAS dimerizes with Arnt (Fig. 1D, left). To further delineate the function of NEPAS, expression vectors of HIF-1α and HIF-2α were transfected into 293T cells concomitant with a luciferase (Luc) reporter driven by HRE and either NEPAS or HIF-3α cDNA (Fig. 1D, middle). HIF-1α and HIF-2α strongly enhanced reporter gene expression. Further enhancement of reporter gene expression was observed following exposure to $CoCl_2$, which mimics hypoxia through the inhibition of proline hydroxylases. Cotransfection of NEPAS cDNA suppressed the HIF-1α/HIF-2α-induced expression of HRE reporter gene expression both during normoxia and in the presence of $CoCl_2$, indicating that NEPAS acts as a negative regulator of HIF-1α and HIF-2α. Expression of an excess amount of Arnt reversed the NEPAS-mediated suppression of reporter gene expression stimulated by HIF-1α or HIF-2α (Fig. 1D, middle), suggesting that NEPAS competes with HIF-1α/HIF-2α for the limited amount of Arnt available. Since NEPAS has an N-terminal transactivation domain like HIF-3α (11, 18), NEPAS retains a weak transactivational activity, which is approximately 1/10 of the activity of HIF-1α and HIF-2α (Fig. 1D, middle and right).

Expression analysis of NEPAS. Gene expression analysis by RT-PCR revealed that NEPAS mRNA is broadly expressed in various tissues of the mouse during the embryonic and neonatal stages and that NEPAS expression gradually decreases toward P15 (Fig. 2A, top). In adult mice, the expression of NEPAS was barely detectable during normoxia. In contrast, IPAS mRNA was not detected in embryos (data not shown). The HIF-3α transcript was expressed in virtually all the embryonic and adult tissues examined (Fig. 2A, middle). These results thus demonstrate that the expression levels of NEPAS, IPAS, and HIF-3α vary substantially during the developmental stage.

Generation of *NEPAS*/*HIF-3α* gene-knockout mice. To investigate the physiological significance of the expression of NEPAS and HIF-3α in the embryo, we generated mice lacking a common exon for the two transcripts. The exon encoding the bHLH domain of the murine *NEPAS*/*HIF-3*α gene was disrupted by replacing it with GFP and a neomycin resistance cDNA cassette (Fig. 2B). We generated mutant ES cells by means of a standard homologous recombination procedure. Two isolated mutant ES cells with a disrupted *NEPAS*/*HIF-3*α allele successfully passed through the germ line (Fig. 2C). Male and female heterozygous mutant mice were intercrossed, and

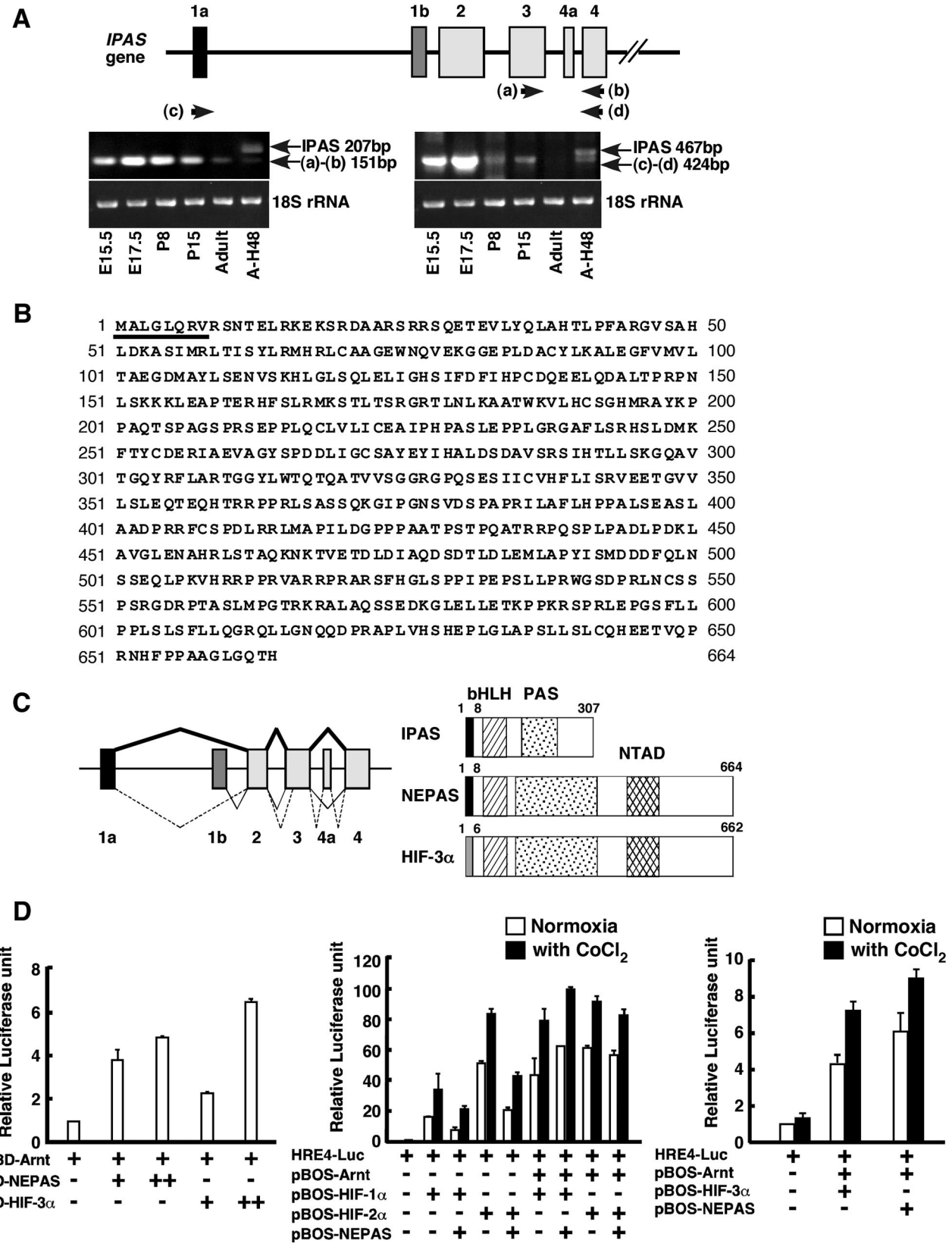

FIG. 1. NEPAS is a bHLH/PAS domain protein. (A) RT-PCR analysis of IPAS mRNA expression in the lung. RNA was purified from wild-type lung at various developmental stages: E15.5, E17.5, P8, P15, adult mouse, and hypoxia-treated adult mouse (A-H48; 6% O_2 for 48 h). The primers used are indicated with arrows (a to d). The 151-bp band (primer set a-b) was the same size as HIF-3α, whereas the 424-bp band (primer set c-d) was an unexpected size. (B) Amino acid sequence of NEPAS. Underlined amino acids are different from those of HIF-3α. (C) Comparison of NEPAS, IPAS, and HIF-3α showing each splicing pattern (NEPAS, thick line; IPAS, dashed line; HIF-3α, thin line) and the primary structures. (D) GAL4 two-hybrid assay

homozygous mutant mice were obtained at the expected Mendelian ratio (24.8%; 366 mice analyzed). Newborn mutant mice appeared outwardly normal and were viable and fertile. GFP signals from the knocked-in allele displayed a ubiquitous expression profile in heterozygous and homozygous mutant embryos, with robust expression in vessels at E8.5 and in heart at E13.5 (Fig. 2D). This is consistent with the observation that NEPAS and HIF-3α mRNAs were expressed throughout embryonic development (Fig. 2A). Macroscopic observation and histological examination by hematoxylin-eosin staining further demonstrated that *NEPAS/HIF-3α*$^{-/-}$ embryos displayed no apparent morphological abnormality at E13.5 compared to wild-type embryos (Fig. 2D and data not shown).

Phenotypes of *NEPAS/HIF-3α*$^{-/-}$ mice. Macroscopic and microscopic analyses of E15.5 *NEPAS/HIF-3α*$^{-/-}$ embryos revealed that there was no apparent difference between wild-type embryonic heart and mutant mouse embryonic heart (data not shown). However, as shown in the left panels of Fig. 3A, E17.5 *NEPAS/HIF-3α*$^{-/-}$ mutant embryonic heart (bottom panel) displayed a slight enlargement of the right atrium (RA) and RV compared with those of wild-type embryos (top panel). At P8 (Fig. 3A, middle) and P15 (data not shown), enlargement of the RV became prominent in *NEPAS/HIF-3*$^{-/-}$ mouse heart. In adult *NEPAS/HIF-3α*$^{-/-}$ mutant mice the enlargement of RA and RV continued, but it was also noted that the RV wall did not show apparent hypertrophy (Fig. 3A, right). The measurements of RV dimensions showed that the difference between wild-type mouse heart ($4.67 \pm 0.648/mm^2$ [$n = 8$]) and *NEPAS/HIF-3α*$^{-/-}$ mouse heart ($6.83 \pm 0.738/mm^2$ [$n = 7$]) was statistically significant ($P < 0.001$; Fig. 3B, left). In contrast, no enlargement was observed in the LVs of adult mutant mice (LV dimensions: wild type, $12.1 \pm 2.31/mm^2$ [$n = 8$], versus *NEPAS/HIF-3α*$^{-/-}$, $12.9 \pm 2.61/mm^2$ [$n = 7$] [Fig. 3B, middle]).

As shown in the right panel of Fig. 3B, the RV blood pressure in adult mice was significantly lower in the *NEPAS/HIF-3α*$^{-/-}$ mutant mice (18.1 ± 1.97/mm Hg [$n = 9$]) than in the wild-type mice (22.4 ± 2.06/mm Hg [$n = 7$]; $P = 0.006$). We speculated that the mutant RA began dilation in the early stages of heart development. The loss of elasticity in the mutant heart is considered to be a cause of low RV blood pressure in the adult. Despite this impairment of heart function, we have not seen the *NEPAS/HIF-3α*$^{-/-}$ mutant mice die because of heart failure under normal circumstances. The homozygous mutant mice lived relatively long (data not shown), indicating that the heart phenotype is not immediately fatal.

Since a lack of desmin expression has been reported to cause cardiomyocyte hypertrophy and heart dilation (35), we examined the expression of desmin in the heart by immunostaining. Although intermediate filaments positive for desmin localized along the Z-disks in striated muscle fibers of wild-type and mutant hearts, there was an extreme disarrangement of striated muscle fibers observed in *NEPAS/HIF-3α*$^{-/-}$ mutant hearts, indicative of muscle degeneration (Fig. 3C, top). However, massive fibrosis of the RV wall, characteristic of right ventricular dysplasia, was not observed in *NEPAS/HIF-3α*$^{-/-}$ hearts. Furthermore, the expression of brain natriuretic peptide mRNA, known to be elevated in cardiomyopathy (32), was normal in the mutant RV (data not shown). Hence, the available lines of evidence do not support the contention that cardiomyopathy is the cause of RV enlargement in *NEPAS/HIF-3α*$^{-/-}$ mice.

In contrast, we found an excess number of CD31-positive microcapillaries in the myocardium of the *NEPAS/HIF-3α*$^{-/-}$ heart (Fig. 3C, bottom) and suspect this to be the cause of the irregular array of striated muscle fibers in the *NEPAS/HIF-3α*$^{-/-}$ myocardium (Fig. 3C, top). This compelled us to investigate the expression of vascular endothelial growth factor (VEGF) and VEGF receptors as a possible cause of endothelial cell proliferation in ischemic and hypoxic preconditioning of the heart (20). However, the expression of $VEGF_{164}$ and its receptors Flk-1 and Flt-1 was unaffected in the *NEPAS/HIF-3α*$^{-/-}$ heart (data not shown).

Impaired pulmonary remodeling in *NEPAS/HIF-3α*$^{-/-}$ mice. Since NEPAS mRNA is highly expressed in the embryonic and neonatal lungs and since pulmonary remodeling and pulmonary hypertension are often associated with RV enlargement, we also performed histological examination of the *NEPAS/HIF-3α*$^{-/-}$ mouse lungs. The airspace walls were getting thicker in the wild-type lungs as mice grew from P2 through P15 (Fig. 3D and E), at which time secondary septa incompletely partitioned the smooth channels and saccules (3). In the *NEPAS/HIF-3α*$^{-/-}$ lung, we found that the walls of secondary septa have subdivided alveoli (Fig. 3D and E), implying that the process of alveolar formation advances more rapidly than in the wild-type lung. In addition, incomplete alveolar spaces have been occasionally observed in P15 and adult *NEPAS/HIF-3α*$^{-/-}$ mutant lungs (Fig. 3E). Immunostaining of alveolar endothelial cells with an anti-CD31 antibody revealed the defective space increase in interalveolar septa and hyperplasia of endothelial cells in the *NEPAS/HIF-3α*$^{-/-}$ lung during maturation of alveolar formation (Fig. 3E).

We also examined the embryonic lungs. In E17.5 wild-type mice, epithelial tubes extended into, and capillary networks developed within, the mesenchyme (data not shown). In contrast, a reduction in the mesenchyme was observed in E17.5 *NEPAS/HIF-3α*$^{-/-}$ lung and CD31-positive endothelial cells surrounded the epithelial tubes at the time, suggesting that the excessive development of lung remodeling begins in the lung of *NEPAS/HIF-3α*$^{-/-}$ embryos (data not shown).

Since HIF-1α and HIF-2α are involved in the remodeling of pulmonary arterioles (2, 4, 30), we further investigated muscularized vessels in alveoli and alveolar ducts by elastin fiber staining in P8 and adult mouse lungs. Victoria blue-van Gieson

in 293T cells under normoxic conditions. Note that NEPAS interacts with Arnt (left). NEPAS inhibits reporter gene activation by HIFs under normoxic conditions (white bars) or after exposure to $CoCl_2$ (black bars) (middle). The NEPAS-Arnt heterodimer has a weak transactivation activity under normoxic conditions (white bars) or after exposure to $CoCl_2$ (black bars) (right). Data are presented as induction (*n*-fold) relative to cells transfected with reporter plasmid alone, defined as 1. Note the difference in magnitude of transactivation in the middle and right panels. The error bars represent means ± standard deviations.

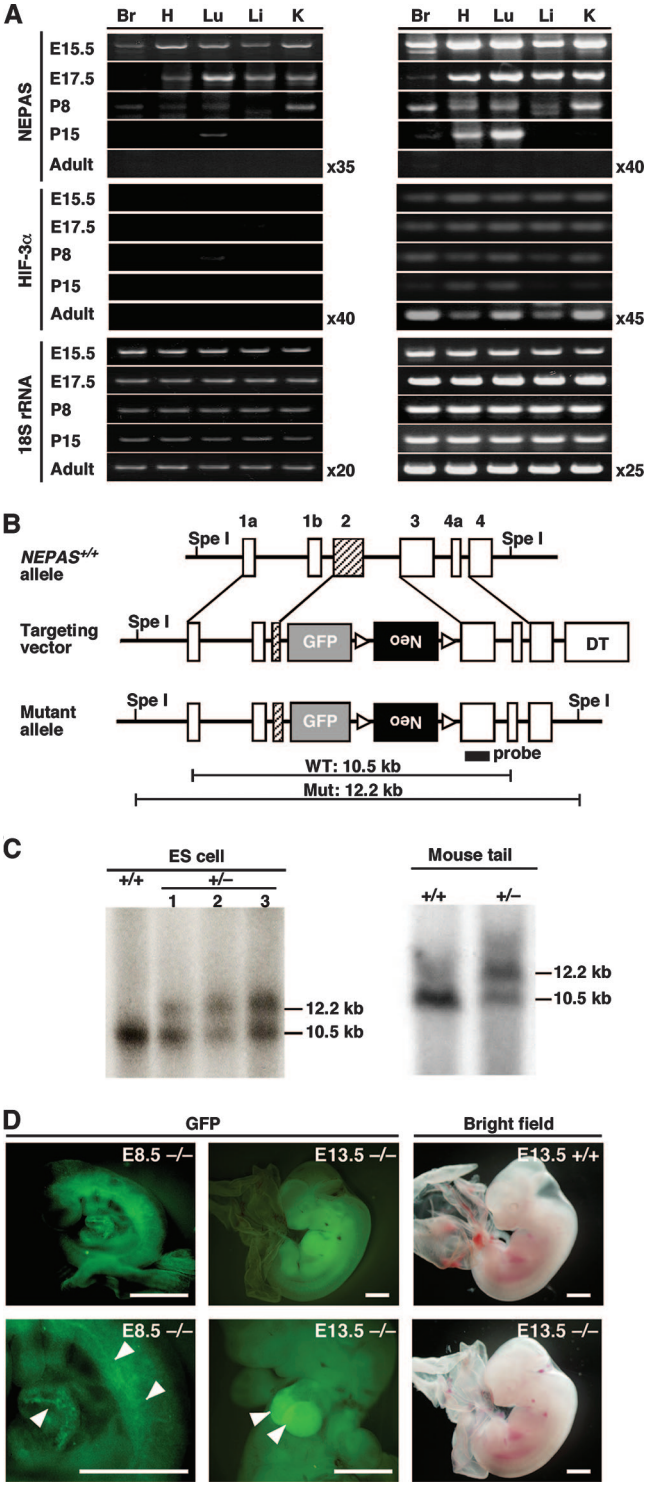

FIG. 2. Targeted disruption of *NEPAS/HIF-3α* gene. (A) RT-PCR analysis of NEPAS and HIF-3α expression in various mouse tissues at different stages. Br, brain; H, heart; Lu, lung; Li, liver; K, kidney. As an internal control, 18S rRNA was used. (B) *NEPAS/HIF-3α* targeting construct. Top, map of the murine *NEPAS* gene; middle, structure of the *NEPAS* targeting construct containing a neomycin resistance gene (*Neo*), a green fluorescent protein gene (*GFP*), and a diphtheria toxin gene (*DT*); bottom, structure of the targeted *NEPAS/HIF-3α* allele that results in insertion of the *Neo* and *GFP* genes within the bHLH domain. The black bar represents the hybridization probe used for Southern blot analysis. (C) Southern blot analysis of SpeI-digested genomic DNA from ES cell clones (left) and mouse tails (right). The 10.5-kb band corresponds to the wild-type *NEPAS* allele/*HIF-3α*, whereas the 12.2-kb band corresponds to the homologous recombined allele. (D) Macroscopic examination of E8.5 and E13.5 embryos by fluorescent field and E13.5 embryos by bright-field microscopy. The genotypes of each image were either wild type (+/+) or *NEPAS/HIF-3α*$^{-/-}$ (−/−). Note that GFP was expressed in the entire *NEPAS/HIF-3α*$^{-/-}$ embryonic body and was strongly expressed in vessels (E8.5, arrowheads) and heart (E13.5, arrowheads). Bars, 1 mm (E13.5) and 0.5 mm (E8.5).

staining was performed for the detection of elastic fibers surrounding vessels in the *NEPAS/HIF-3α*$^{-/-}$ lung at P8 (Fig. 3F). Elastic fibers were stained blue in this analysis. The vessels in the lung and less than 30 μm in diameter were divided into three categories: (i) vessels with a single elastin fiber (SEF) (vessels were surrounded by single elastic lamina [Fig. 3F, left]), (ii) vessels with partially multiple elastin fiber (PEF) (vessels were surrounded by internal elastic lamina and in part by external lamina [Fig. 3F, middle]), and (iii) vessels with fully multiple elastin fiber (MEF) (vessels were surrounded fully by internal and external elastic lamina [Fig. 3F, right]).

We scored the frequency of these three types of vessels. Compared to wild-type mice, MEF vessels developed more frequently in both P8 and adult *NEPAS/HIF-3α*$^{-/-}$ mutant lungs, with a wall thickness comparable to that of the wild type (Fig. 3G). SEF vessels decreased accordingly. We also investigated muscularized vessels in P8 and adult lungs by immunostaining with anti-smooth muscle cell (SMC) actin antibody. In the mutant lungs, the frequency of fully muscularized vessels surrounded by SMC was comparable to that of the wild type (data not shown). Similarly, there was no significant difference between mutant and wild-type mouse lungs in the wall thickness of fully muscularized vessels. These results are in contrast to those reported previously for adult wild-type mice exposed to hypoxia (10% oxygen) for 4 weeks (2), probably due to the short period of ischemic exposure during *NEPAS/HIF-3α*$^{-/-}$ mouse development.

Coexpression of NEPAS and HIF-2α. Since expression of the *GFP* gene knocked into the *NEPAS* locus faithfully recapitulated the expression of NEPAS, we examined cellular localization of NEPAS in the lung of *NEPAS/HIF-3α*$^{-/-}$ mice at P15 by immunohistochemical analysis using an anti-GFP antibody (Fig. 4A, top right). Normal rabbit IgG was used as a negative control (Fig. 4A, top left). Staining with the anti-GFP antibody was found in the endothelial cells of vessels and capillaries in alveoli of the *NEPAS/HIF-3α*$^{-/-}$ mouse lung. Importantly, the pattern of GFP (i.e., NEPAS) expression was found to colocalize with HIF-2α expression, which was detected in the lung of wild-type and mutant mice at P15 during normoxia by immunostaining with an anti-HIF-2α antibody (Fig. 4A, middle). We also performed immunostaining of the mutant and wild-type lungs using anti-CD31 antibody (Fig. 4A, bottom). The expression of CD31 overlapped with the GFP expression.

The lungs were also stained with anti-SP-D antibody, which stains type II alveolar cells (4). Staining with anti-SP-D antibody appeared to be positive for the cells that were positive for anti-GFP antibody in the *NEPAS/HIF-3α*$^{-/-}$ mouse lung in

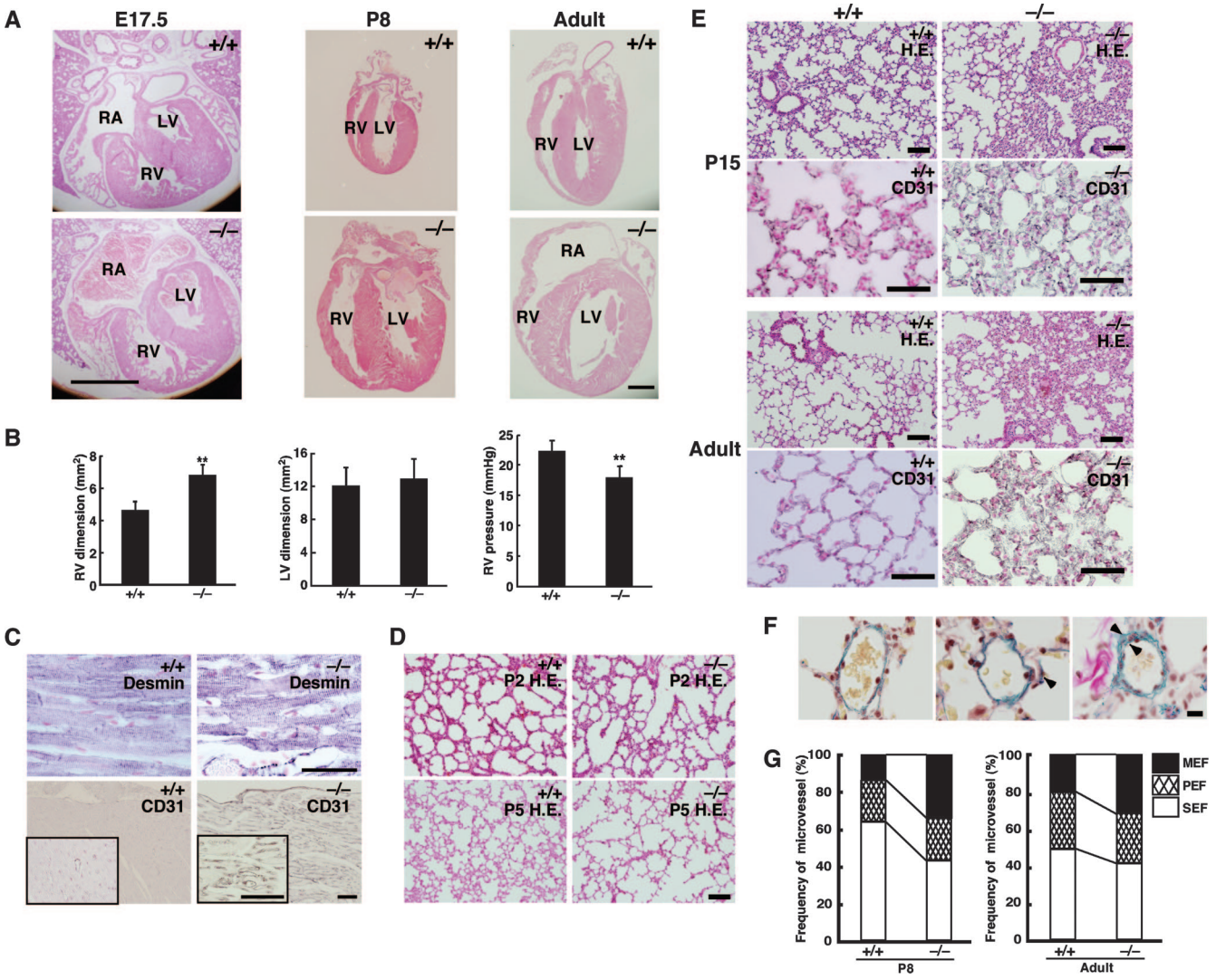

FIG. 3. Impaired heart and lung development in *NEPAS/HIF-3α*$^{-/-}$ mice. (A) Hematoxylin-eosin staining of sections from wild-type mice (top) and *NEPAS/HIF-3α*$^{-/-}$ mice (bottom) at E17.5, P8, and adult stage showing enlargement of the right sides of *NEPAS/HIF-3α*$^{-/-}$ hearts. Bars, 0.1 mm (E17.5) and 1 mm (P8 and adult). (B) Histograms of RV and LV dimensions and RV blood pressure obtained by echo analysis of seven or eight mice (mean ± standard deviation). **, $P < 0.01$. (C) Immunostaining of adult wild-type and *NEPAS/HIF-3α*$^{-/-}$ hearts with antidesmin and anti-CD31 antibodies. Black staining represents positive signals. Note the irregular striated muscle fibers and large number of microcapillaries in the myocardium of the *NEPAS/HIF-3α*$^{-/-}$ heart. Bars, 100 μm (CD31) and 50 μm (desmin). (D) Hematoxylin-eosin (H.E.)-stained P2 (top) and P5 (bottom) lung sections of wild-type (left) and *NEPAS/HIF-3α*$^{-/-}$ (right) mice. Bar, 100 μm. (E) Hematoxylin-eosin (H.E.)-stained and CD31-immunostained P15 (top four panels) and adult (bottom four panels) lung sections. Note the incomplete alveolar spaces surrounded by CD31-positive endothelial cells (black staining) in *NEPAS/HIF-3α*$^{-/-}$ lung at both P15 and the adult stage. Bars, 100 μm (hematoxylin-eosin staining) and 50 μm (CD31). (F) Victoria blue-van Gieson staining for the detection of elastic fibers surrounding vessels in *NEPAS/HIF-3α*$^{-/-}$ lung at P8. Elastic fibers were stained blue and classified as SEF-containing vessels (left), PEF-containing vessels (middle), or fully MEF-containing vessels (right). Bar, 10 μm. (G) Comparison of the frequency of SEF (white bars), PEF (crosshatched bars), and MEF (black bars) in P8 and adult lungs between wild-type and *NEPAS/HIF-3α*$^{-/-}$ mice. Note that the number of vessels <30 μm in diameter, classified as MEF, per 100 alveoli in both P8 and adult *NEPAS/HIF-3α*$^{-/-}$ lungs increased significantly ($P < 0.01$).

consecutive sections (Fig. 4B), indicating that the expression of NEPAS overlaps with that of SP-D in alveolar epithelium. In contrast, only weak HIF-1α immunostaining was seen in SMCs lining the vessels in the lung under conditions of normoxia (data not shown), in agreement with the previous report that HIF-1α protein is only modestly expressed in lung SMCs during normoxia (26, 30).

Enhanced expression of ET-1 in NEPAS/HIF-3α-null lung. It has been reported that ET-1 and PDGF-β expression levels increase in mouse lungs after prolonged exposure to hypoxia, resulting in pulmonary hypertension and enlargement of the RV (5, 16, 28). We therefore speculated that enhanced expression of these mediators might be associated with the defects in heart development and lung remodeling in *NEPAS/HIF-3α*$^{-/-}$ mutant mice. Therefore, we examined the expression of these factors by RT-PCR. ET-1 mRNA expression in the lung and heart of the null mutant was similar to that of the wild type at E15.5 and increased approximately fourfold at E17.5 (data not shown). On the other hand, PDGF-β mRNA expression was not affected in the mutant mouse embryos. Under normoxic

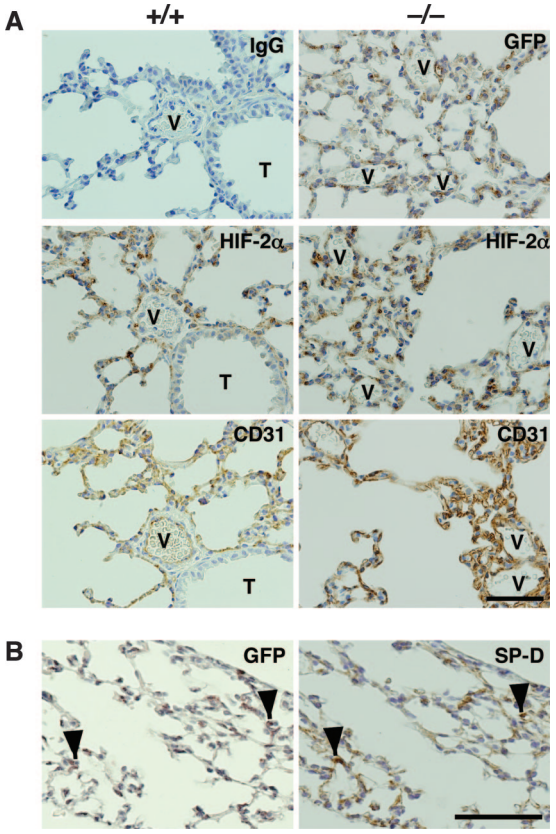

FIG. 4. Coexpression of NEPAS and HIF-2α. (A) Immunostaining of *NEPAS/HIF-3α*$^{-/-}$ (−/−) and wild-type (+/+) lungs at P15 using anti-HIF-2α, anti-CD31, and anti-GFP antibodies. Normal rabbit IgG was used as a negative control (top left). Positive immunostaining signals are brown. Anti-GFP antibody staining of wild-type mouse lung is similar to that of the normal IgG control (data not shown). Note the colocalization of HIF-2α and GFP expression in vascular endothelium. V, vessel; T, trachea. (B) Immunostaining of *NEPAS/HIF-3α*$^{-/-}$ and wild-type lungs at P15 using anti-SP-D and anti-GFP antibodies. SP-D is a marker of type II alveolar cells. Note the colocalization of SP-D and GFP expression in alveolar epithelium (arrowheads). Bar, 50 μm.

conditions, ET-1 mRNA expression was elevated in P15 *NEPAS/HIF-3α*$^{-/-}$ mutant mouse lungs at P15 but not in heart. PDGF-β mRNA was increased in P15 *NEPAS/HIF-3α*$^{-/-}$ mouse heart, suggesting that PDGF-β is involved in the increased formation of microcapillaries in the *NEPAS/HIF-3α*$^{-/-}$ myocardium.

These alterations in gene expression were confirmed by fluorescence-activated cell sorting (FACS) analysis of isolated lung endothelial cells from P8 mutant mice (Fig. 5A). Lung cells in the rectangles in Fig. 5A designated R1 and R2 (wild-type mice) and R3, R4, and R5 (*NEPAS/HIF-3α*$^{-/-}$ mutant mice) were harvested for RT-PCR analyses. ET-1, PDGF-β, and HIF-2α mRNA expression levels were approximately threefold higher in the R3 fraction (CD31$^+$/GFP$^+$) of mutant mice than in the R1 fraction (CD31$^+$/GFP$^-$) of wild-type mice (Fig. 5B). In contrast, the expression levels of HIF-1α, $VEGF_{164}$, and the VEGF receptors Flk-1 (Fig. 5B) and Flt (data not shown) were not affected substantially.

The expression of ET-1 protein was measured by means of ELISA in *NEPAS/HIF-3α*$^{-/-}$ and wild-type lung endothelial

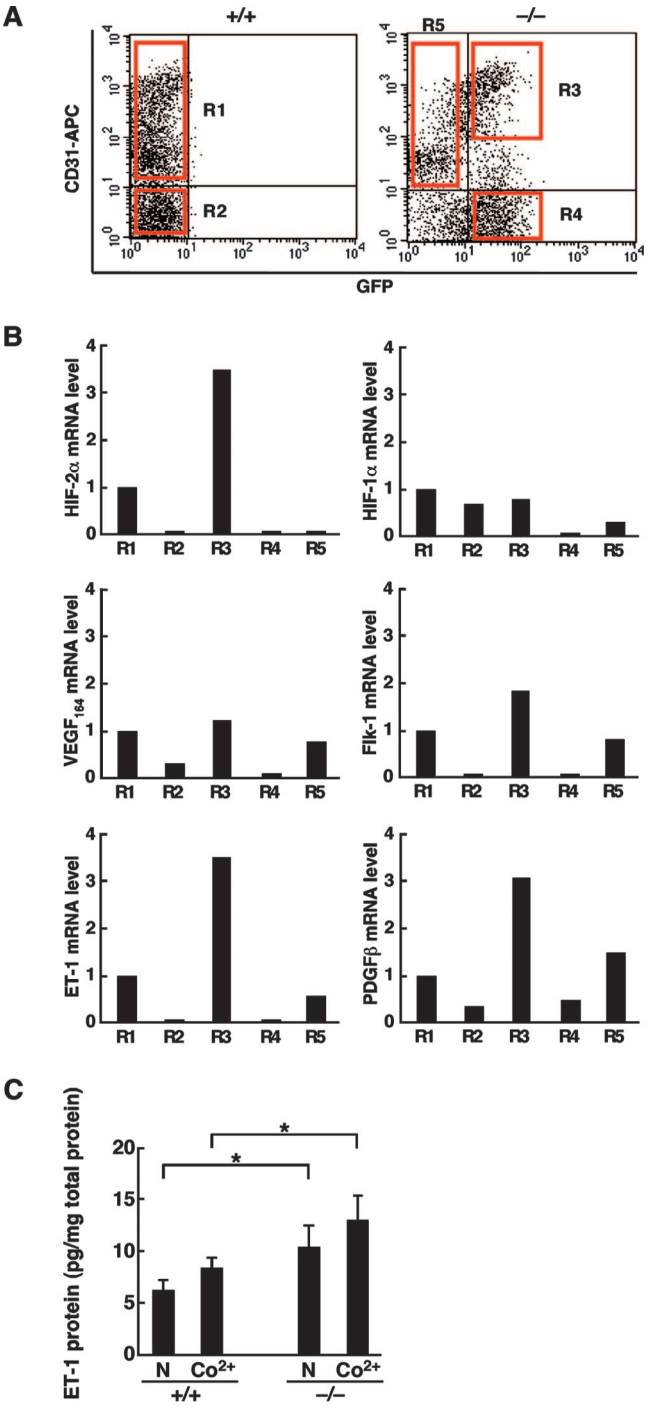

FIG. 5. Elevated ET-1 expression in *NEPAS/HIF-3α*$^{-/-}$ lung endothelial cells. (A) FACS sorting of lung endothelial cells from wild-type (left) and *NEPAS/HIF-3α*$^{-/-}$ (right) mice at P8. Lung cells in the rectangles designated R1 and R2 (wild type) and R3, R4, and R5 (*NEPAS/HIF-3α*$^{-/-}$ mice) were harvested for RT-PCR analyses. R1, CD31$^+$/GFP$^-$; R2, CD31$^-$/GFP$^-$; R3, CD31$^+$/GFP$^+$; R4, CD31$^-$/GFP$^+$; R5, CD31$^+$/GFP$^-$. APC, allophycocyanin. (B) RT-PCR analyses of the mRNA expression of HIF-2α, HIF-1α, $VEGF_{164}$, Flk-1, ET-1, and PDGF-β in R1 to R5 fractions. Data are presented relative to the internal control 18S rRNA expression levels. The R1 data were set to 1. (C) Expression of ET-1 protein examined by ELISA in lung endothelial cells of wild-type and *NEPAS/HIF-3α*$^{-/-}$ mice. ET-1 expression was analyzed under normoxic conditions (N) or in the presence of $CoCl_2$ (Co^{2+}). *, $P < 0.05$.

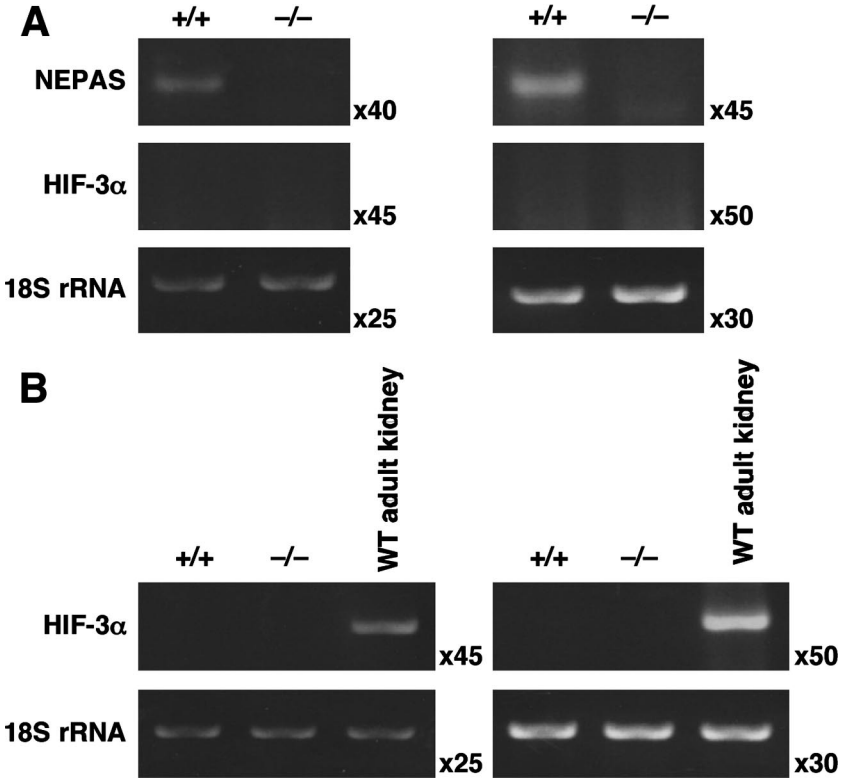

FIG. 6. RT-PCR analysis of NEPAS mRNA expression in lung endothelial cells at P8. (A) FACS-sorted lung endothelial cells from wild-type (+/+) and *NEPAS/HIF-3*$\alpha^{-/-}$ (−/−) mice at P8 were immortalized and examined for the expression of NEPAS or HIF-3α. (B) RT-PCR analysis of HIF-3α mRNA expression utilizing primer sets different from those used in panel A. Note that wild-type lung endothelial cells at P8 barely expressed HIF-3α, while NEPAS was abundantly expressed. WT, wild type.

cells (Fig. 5C). Consistent with the mRNA analysis, the ET-1 protein in cytosol extracts was clearly higher in *NEPAS/HIF-3*$\alpha^{-/-}$ lung endothelial cells than in wild-type lung endothelial cells under normoxic conditions (1.7-fold). Similarly, the ET-1 protein level was higher in *NEPAS/HIF-3*$\alpha^{-/-}$ lung endothelial cells than in wild-type cells in the presence of $CoCl_2$ (1.6-fold). Sequence surveys identified an HRE motif in the *ET-1* gene (14) but not in the *PDGF*-β gene, suggesting that *ET-1* gene expression may be regulated directly by the HIF-2α/Arnt heterodimer, whereas *PDGF*-β gene regulation may be complex and remains to be clarified.

Enhanced expression of ET-1 in isolated NEPAS/HIF-3α-null endothelial cells. To further investigate the mechanisms of target gene regulation in lung endothelial cells, we isolated primary P8 lung endothelial cells derived from wild-type and *NEPAS/HIF-3*$\alpha^{-/-}$ mutant mice (CD31-positive R1 and R3 fractions, respectively) and immortalized these cells by transfection with polyomavirus middle T antigen. RT-PCR analyses of the transformed cells using specific sets of primers for NEPAS and HIF-3α showed predominant expression of the NEPAS transcript in wild-type endothelial cells (Fig. 6A). In contrast, a very low level of expression of HIF-3α mRNA was observed in these cells (Fig. 6B). These results support our contention that NEPAS is predominantly expressed in P8 mouse lung endothelial cells.

RT-PCR data for ET-1 and VEGF mRNA expression in *NEPAS/HIF-3*$\alpha^{-/-}$ and wild-type lung-derived endothelial cells under normoxic conditions and after exposure to $CoCl_2$ are shown in the left panel of Fig. 7A. In the right panel relative increases of ET-1 and VEGF mRNA are shown. The expression of ET-1 mRNA in *NEPAS/HIF-3*$\alpha^{-/-}$ cells was approximately fourfold higher than that of the wild-type cells during normoxia. Upon exposure to $CoCl_2$ the expression of ET-1 mRNA in wild-type cells was increased to a level similar to that of *NEPAS/HIF-3*$\alpha^{-/-}$ cells. Since there was no further increase in ET-1 mRNA expression in *NEPAS/HIF-3*$\alpha^{-/-}$ cells by $CoCl_2$ treatment, the expression of ET-1 mRNA seems to be fully activated in the mutant cells. In contrast, VEGF mRNA was elevated only slightly (less than twofold) in both wild-type and mutant cells in response to $CoCl_2$ treatment. The expression of NEPAS was upregulated in the wild-type endothelial cells after exposure to $CoCl_2$ (Fig. 7A, left). Taken together, these results suggest that the expression levels of VEGF and ET-1 are differentially regulated by HIF family transcription factors, although they have similar HRE sequence motifs in their promoters.

To investigate the function of NEPAS in endothelial cells, a NEPAS expression vector was transfected into the lung endothelial cells of wild-type and mutant mice and the expression levels of ET-1, VEGF, and NEPAS mRNAs were monitored by RT-PCR (Fig. 7B, left). In the right panel of Fig. 7B relative increases of ET-1 and VEGF mRNAs are shown. Transfection with the NEPAS expression vector markedly inhibited ET-1 mRNA expression in *NEPAS/HIF-3*$\alpha^{-/-}$ cells, whereas it was

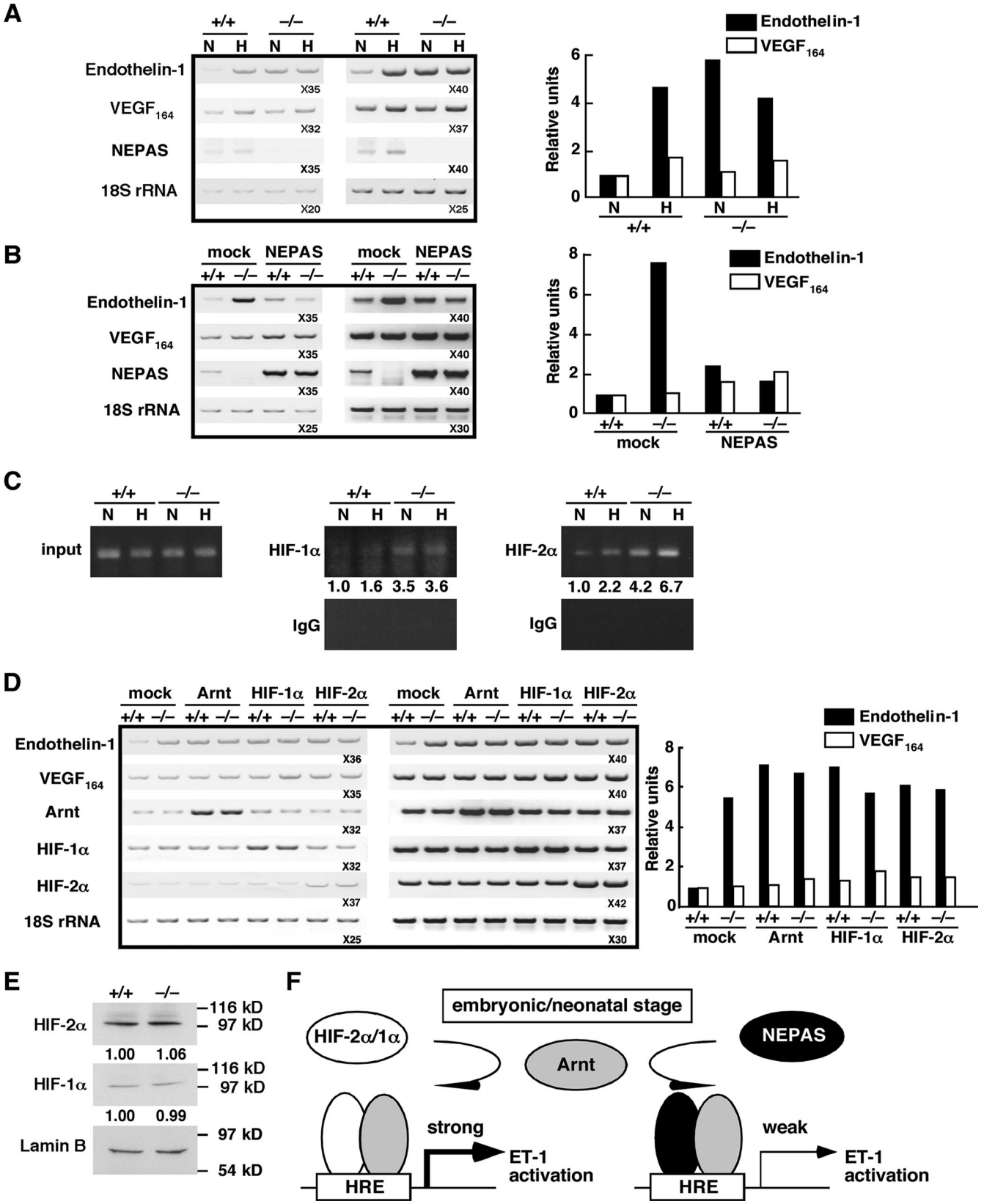

FIG. 7. Enhanced ET-1 expression in *NEPAS/HIF-3α*$^{-/-}$ lung endothelial cells under normoxic conditions. (A) RT-PCR analysis of ET-1 (black bars) and VEGF (white bars) expression in wild-type and *NEPAS/HIF-3α*$^{-/-}$ lung-derived endothelial cells under normoxic conditions (N) and after exposure to $CoCl_2$ (H). (B) Transfection of NEPAS into *NEPAS/HIF-3α*$^{-/-}$ cells revealing significant suppression of ET-1 expression. (C) ChIP assay using anti-HIF-1α and anti-HIF-2α antibodies on wild-type and *NEPAS/HIF-3α*$^{-/-}$ lung endothelial cells under

not much affected or was even slightly increased by the treatment in wild-type cells. In contrast, VEGF mRNA expression was only marginally increased in wild-type and mutant cells, consistent with the notion that *ET-1* gene expression and *VEGF* gene expression are differentially regulated. A slight increase in the expression of VEGF mRNA could be explained by the overexpression of NEPAS having a weak transactivating activity. PDGF-β was weakly expressed in isolated lung endothelial cells from wild-type and mutant mice, and the expression was not significantly affected following transfection with the NEPAS expression vector (data not shown). While this contrasts with our previous results, this may indicate that PDGF-β expression was locally different in alveoli compared with ET-1 expression in endothelial cells and that its enhanced expression may not be directly involved in pulmonary vascular remodeling.

ChIP analysis revealed that HIF-1α and HIF-2α specifically bound the HRE sequence in the *ET-1* promoter in wild-type cells under hypoxic conditions (Fig. 7C). Importantly, that binding increased in *NEPAS/HIF-3*$\alpha^{-/-}$ cells under normoxic and hypoxic conditions. Based on these findings, we propose that NEPAS/HIF-3α influences the *ET-1* gene transcription by regulating the binding of HIF-1α and HIF-2α to the HRE sequence in the gene.

In agreement with our conclusion in the previous section that a limited amount of Arnt is critical for transcriptional inhibition by NEPAS, transfection of an Arnt expression vector enhanced the expression of ET-1 mRNA in isolated wild-type endothelial cells to the level of its NEPAS/HIF-3α-null counterpart (Fig. 7D). Transfection of HIF-1α or HIF-2α into lung endothelial cells also induced the *ET-1* gene expression to the level of the NEPAS/HIF-3α-null counterpart. However, VEGF mRNA expression was not affected in either wild-type or NEPAS/HIF-3α-null cells by transfection with Arnt, HIF-1α, or HIF-2α (Fig. 7D).

Immunoblot analysis revealed that HIF-2α and HIF-1α expression levels were similar both in wild-type and in NEPAS/HIF-3α-null mutant cells, although HIF-2α was much more abundant than HIF-1α (Fig. 7E). HIF-2α and HIF-1α protein levels were unchanged in endothelial cells under hypoxic conditions (data not shown). These results are consistent with our conclusion that under normoxic conditions, distinct regulatory mechanisms determine the transcriptional activity of HIF without altering HIF-2α or HIF-1α protein levels in endothelial cells.

DISCUSSION

Since the amount of oxygen supplied from maternal blood to embryos through placenta is limited, embryos are continuously exposed to lower oxygen tension (9). Neonates are suddenly exposed to high oxygen tension at birth, when spontaneous breathing begins. Development of the cardiorespiratory system is necessary to adapt to this dramatic change in the oxygen availability during the perinatal period. In this study we found that a novel splicing variant product of the *HIF-3*α gene, NEPAS, is predominantly expressed during embryonic and neonatal stages and acts as a negative regulator of HIF transcription factor-mediated gene expression. We found that *NEPAS/HIF-3*$\alpha^{-/-}$ mice show impaired lung remodeling at the late embryonic stage, which results in right ventricular enlargement in the adult stage. This observation indicates that the NEPAS/HIF-3α transcription factors play essential roles in the development of the cardiorespiratory system. This negative regulation by NEPAS of HIF-1α and -2α activity offers an important stage-specific regulation of the development of the cardiorespiratory system (29) and underscores the complexity of the regulatory mechanisms controlling the function of HIF transcription factors as well as their target physiological processes.

Whereas both HIF-3α and IPAS are known to work as negative regulators of HIF-1α and -2α (11, 19), this study has unequivocally proven that endothelial cells derived from the lungs of embryos and juvenile mice predominantly express NEPAS. We found that NEPAS is expressed during embryonic and neonatal stages, while HIF-3α is stably expressed in the adult stage. This difference in expression profiles is mediated by the differential use of exons 1a and 1b. Several HREs reside in the promoter upstream region of exon 1a, but not in the upstream region of exon 1b. Indeed, when we subjected embryos and neonates to hypoxia, we found that NEPAS is induced by hypoxia but HIF-3α is not (data not shown). We also found that the IPAS form of the exon 1a splicing variant appears at a much later stage than NEPAS does during mouse development, suggesting that the observed heart and lung defects can be attributed solely to the inactivation of NEPAS. The latter observation further suggests that the difference in the splicing regulation is critical for the biological function of NEPAS and HIF-3α and that the molecular basis of the regulation has to be elucidated.

One remaining possibility is that since IPAS is a hypoxia-inducible protein, it may be locally induced during embryonic development. Therefore, we cannot rule out entirely the possibility that IPAS is working as a negative regulator in the local area (i.e., lung and heart) in an early developmental stage. In contrast, whereas the N-terminal 8-amino-acid sequences are encoded by the respective first exons of NEPAS and HIF-3α, we envisage that their contribution to the distinct biological functions may not be significant.

It should be noted that, in addition to the difference in alternative splicing, a difference in selecting their partner molecules to form a heterodimer between HIF-3α/NEPAS and IPAS seemingly contributes to the establishment of their unique regulatory features. This mechanism is depicted in Fig. 7F. HIF-3α and NEPAS dimerize with the common partner molecule Arnt, which decreases the HIF-1α–Arnt and HIF-

normoxic conditions (N) or in the presence of $CoCl_2$ (H). Normal mouse IgG or rabbit IgG was used as a negative control. (D) Transfection of Arnt, HIF-1α, or HIF-2α into lung endothelial cells revealing induction of ET-1 (black bars) but not VEGF (white bars) expression. (E) Western blot analysis of wild-type and *NEPAS/HIF-3*$\alpha^{-/-}$ cells showing the expression of HIF-2α (top), HIF-1α (middle), and control lamin B (bottom). (F) Model illustrating the effect of NEPAS on ET-1 regulation during embryonic and neonatal stages.

2α–Arnt levels. Because both HIF-3α and NEPAS lack the CTAD, the activation of target gene transcription by HIF-3α–Arnt and NEPAS-Arnt is much weaker than that by HIF-1α–Arnt or HIF-2α–Arnt. Thus, HIF-3α and NEPAS compete with HIF-1α and HIF-2α and repress the cellular response to hypoxia. In contrast, IPAS interacts directly with HIF-α factors in replacing Arnt (19). Because the HIF-α–IPAS heterodimer is unable to bind DNA, IPAS can completely repress activity of HIF-1α and HIF-2α. This distinct mechanism seems to be a key to unraveling the functional contributions of these negative regulators of HIFs to developmental and adult physiology.

Our gene targeting study revealed that abrogation of the NEPAS/HIF-3α function results in defective lung and heart development. Pulmonary hypertension during the developmental stage leads to right ventricular hypertrophy, dilation, and heart failure (26, 28). In the developmental stage of NEPAS/HIF-3α-null mice, RV dilation and hypertrophy were most likely to be due to the pulmonary hypertension. We envisage that these RV defects during the growth process resulted in the RV dysfunction observed in the adult NEPAS/HIF-3α-null mice.

Although some recent experimental models using gene-engineered mice have unraveled some of the cellular and molecular aspects of the pathophysiology of pulmonary hypertension, information remains insufficient for understanding this complex process. Several animal experiments suggested that persistent activation of HIF-1α and HIF-2α plays a key role in causing pulmonary hypertension. HIF-1α and HIF-2α rapidly induce expression of vasodilators and decrease vasoconstrictors and thereby are involved in adaptation of lung endothelial cells to hypoxia (1, 38). However, since this rapid adaptation is incapable of enduring persistent hypoxia, an imbalance between vasodilators and vasoconstrictors gradually arises, which results in impaired lung remodeling and pulmonary hypertension (7, 28).

Inhalation of nitric oxide, a vasodilator, provides a tremendous advance in the treatment of this disease (31, 36), and nitric oxide must be an indispensable player in the pathophysiology of persistent pulmonary hypertension in the newborn (PPHN). Other vasodilators such as prostacyclin and prostaglandin I_2 and vasoconstrictors such as ET-1, angiotensin II, and leukotriene may also be involved in the development of PPHN. Here we demonstrated that levels of ET-1 in endothelial cells are significantly upregulated in *NEPAS/HIF-3α*-knockout mice, indicating that the increased ET-1 expression plays a key role in the pathological condition of PPHN. In fact, previous studies demonstrated that a notably high level of ET-1 is observed in infants with persistent pulmonary hypertension (15, 27). Furthermore, these results suggest a possible genetic link between *NEPAS/HIF-3α* and PPHN in humans (29), although unraveling the genetics of PPHN requires further investigations.

In summary, our results identify NEPAS as a novel HIF-3α splice variant that is a critical negative regulator of HIF-1α and -2α for lung and heart development during the embryonic and neonatal stages. Our data suggest that the three HIF-3α variants, NEPAS, HIF-3α, and IPAS, play distinct roles in regulating functions of HIF-1α and HIF-2α in cell type- and developmental stage-specific manners.

ACKNOWLEDGMENTS

We thank Mitsuyasu Kato for helpful discussion and Tania O'Connor for critical reading of the manuscript. We also thank Naomi Kaneko for technical assistance.

This work was supported in part by grants from the JST-ERATO Environmental Response Project (M.Y.); the Ministry of Education, Science, Sports and Culture (M.Y.); JST-SORST (Y.F.-K.); and the Swedish Research Council and Heart-Lung Foundation (L.P.).

REFERENCES

1. **Asikainen, T. M., A. Ahmad, B. K. Schneider, W. B. Ho, M. Arend, M. Brenner, V. Gunzler, and C. W. White.** 2005. Stimulation of HIF-1α, HIF-2α, and VEGF by prolyl 4-hydroxylase inhibition in human lung endothelial and epithelial cells. Free Radic. Biol. Med. **38:**1002–1013.
2. **Brusselmans, K., V. Compernolle, M. Tjwa, M. S. Wiesener, P. H. Maxwell, D. Collen, and P. Carmeliet.** 2003. Heterozygous deficiency of hypoxia-inducible factor-2α protects mice against pulmonary hypertension and right ventricular dysfunction during prolonged hypoxia. J. Clin. Investig. **111:** 1519–1527.
3. **Burri, P. H.** 1984. Fetal and postnatal development of the lung. Annu. Rev. Physiol. **46:**617–628.
4. **Compernolle, V., K. Brusselmans, T. Acker, P. Hoet, M. Tjwa, H. Beck, S. Plaisance, Y. Dor, E. Keshet, F. Lupu, B. Nemery, M. Dewerchin, P. Van Veldhoven, K. Plate, L. Moons, D. Collen, and P. Carmeliet.** 2002. Loss of HIF-2α and inhibition of VEGF impair fetal lung maturation, whereas treatment with VEGF prevents fetal respiratory distress in premature mice. Nat. Med. **8:**702–710.
5. **Edelberg, J. M., W. C. Aird, W. Wu, H. Rayburn, W. S. Mamuya, M. Mercola, and R. D. Rosenberg.** 1998. PDGF mediates cardiac microvascular communication. J. Clin. Investig. **102:**837–843.
6. **Ema, M., S. Taya, N. Yokotani, K. Sogawa, Y. Matsuda, and Y. Fujii-Kuriyama.** 1997. A novel bHLH-PAS factor with close sequence similarity to hypoxia-inducible factor 1α regulates the VEGF expression and is potentially involved in lung and vascular development. Proc. Natl. Acad. Sci. USA **94:**4273–4278.
7. **Endo, A., M. Ayusawa, M. Minato, M. Takada, S. Takahashi, and K. Harada.** 2001. Endogenous nitric oxide and endothelin-1 in persistent pulmonary hypertension of newborn. Eur. J. Pediatr. **160:**217–222.
8. **Epstein, A. C. R., J. M. Gleadle, L. A. McNeill, K. S. Hewitson, J. O'Rourke, D. R. Mole, M. Mukherji, E. Metzen, M. I. Wilson, A. Dhanda, Y.-M. Tian, N. Masson. D. L. Hamilton, P. Jaakkola, R. Barstead, J. Hodgkin, P. H. Maxwell, C. W. Pugh, C. J. Schofield, and P. J. Ratcliffe.** 2001. *C. elegans* EGL-9 and mammalian homologs define a family of dioxygenases that regulate HIF by prolyl hydroxylation. Cell **107:**43–54.
9. **Genbacev, O., A. Krtolica, W. Kaelin, and S. J. Fisher.** 2001. Human cytotrophoblast expression of the von Hippel-Lindau protein is downregulated during uterine invasion in situ and upregulated by hypoxia in vitro. Dev. Biol. **233:**526–536.
10. **Gu, Y. Z., S. M. Moran, J. B. Hogenesch, L. Wartman, and C. A. Bradfield.** 1998. Molecular characterization and chromosomal localization of third α-class hypoxia inducible factor subunit, HIF-3α. Gene Expr. **7:**205–213.
11. **Hara, S., J. Hamada, C. Kobayashi, Y. Kondo, and N. Imura.** 2001. Expression and characterization of hypoxia-inducible factor (HIF)-3α in human kidney: suppression of HIF-mediated gene expression by HIF-3α. Biochem. Biophys. Res. Commun. **287:**808–813.
12. **Huang, L. E., J. Gu, M. Schau, and H. F. Bunn.** 1998. Regulation of hypoxia-inducible factor 1α is mediated by an O_2-dependent degradation domain via the ubiquitin-proteasome pathway. Proc. Natl. Acad. Sci. USA **95:**7987–7992.
13. **Iyer, N. V., L. E. Kotch, F. Agani, S. W. Leung, E. Laughner, R. H. Wenger, M. Gassmann, J. D. Gearhart, A. M. Lawler, A. Y. Yu, and G. L. Semenza.** 1998. Cellular and developmental control of O_2 homeostasis by hypoxia-inducible factor 1α. Genes Dev. **12:**149–162.
14. **Kakinuma, Y., T. Miyauchi, K. Yuki, N. Murakoshi, K. Goto, and I. Yamaguchi.** 2001. Novel molecular mechanism of increased myocardial endothelin-1 expression in the failing heart involving the transcriptional factor hypoxia-inducible factor-1α induced for impaired myocardial energy metabolism. Circulation **103:**2387–2394.
15. **Kumar, P., N. J. Kazzi, and S. Shankaran.** 1996. Plasma immunoreactive endothelin-1 concentrations in infants with persistent pulmonary hypertension of the newborn. Am. J. Perinatol. **13:**335–341.
16. **Kuwabara, K., S. Ogawa, M. Matsumoto, S. Koga, M. Clauss, D. J. Pinsky, P. Lyn, J. Leavy, L. Witte, J. Joseph-Silverstein, M. B. Furie, G. Torcia, F. Cozzolino, T. Kamada, and D. M. Stern.** 1995. Hypoxia-mediated induction of acidic/basic fibroblast growth factor and platelet-derived growth factor in mononuclear phagocytes stimulates growth of hypoxic endothelial cells. Proc. Natl. Acad. Sci. USA **92:**4606–4610.
17. **Lee, Y. M., C.-H. Jeong, S.-Y. Koo, M. J. Son, H. S. Song, S.-K. Bae, J. A. Raleigh, H.-Y. Chung, M.-A. Yoo, and K.-W. Kim.** 2001. Determination of

hypoxic region by hypoxia marker in developing mouse embryos in vivo: a possible signal for vessel development. Dev. Dyn. **220:**175–186.
18. **Makino, Y., A. Kanopka, W. J. Wilson, H. Tanaka, and L. Poellinger.** 2002. Inhibitory PAS domain protein (IPAS) is hypoxia-inducible splicing variant of the hypoxia-inducible factor-3α locus. J. Biol. Chem. **277:**32405–32408.
19. **Makino, Y., R. Cao, K. Svensson, G. Bertilsson, M. Asman, H. Tanaka, Y. Cao, A. Berkenstam, and L. Poellinger.** 2001. Inhibitory PAS domain protein is negative regulator of hypoxia-inducible gene expression. Nature **414:**550–554.
20. **Maulik, N., and D. K. Das.** 2002. Potentiation of angiogenic response by ischemic and hypoxic preconditioning of the heart. J. Cell. Mol. Med. **6:**13–24.
21. **Maxwell, P. H., M. S. Wiesener, G.-W. Chang, S. C. Clifford, E. C. Vaux, M. E. Cockman, C. C. Wykoff, P. W. Pugh, E. R. Maher, and P. J. Ratcliffe.** 1999. The tumor suppressor protein VHL targets hypoxia-inducible factors for oxygen-dependent proteolysis. Nature **399:**271–275.
22. **Maynard, M. A., H. Qi, J. Chung, E. H. Lee, Y. Kondo, S. Hara, R. C. Conaway, J. W. Conaway, and M. Ohh.** 2003. Multiple splice variants of the human HIF-3α locus are targets of the von Hippel-Lindau E3 ubiquitin ligase complex. J. Biol. Chem. **278:**11032–11040.
23. **Morita, M., O. Ohneda, T. Yamashita, S. Takahashi, N. Suzuki, O. Nakajima, S. Kawauchi, M. Ema, S. Shibahara, T. Udono, K. Tomita, M. Tamai, K. Sogawa, M. Yamamoto, and Y. Fujii-Kuriyama.** 2003. HLF/HIF-2α is key factor in retinopathy of prematurity in association with erythropoietin. EMBO J. **22:**1134–1146.
24. **Ohneda, O., C. Fennie, Z. Zheng, C. Donahue, H. La, R. Villacorta, B. Cairns, and L. A. Laskey.** 1998. Hematopoietic stem cell maintenance and differentiation are supported by embryonic aorta-gonad-mesonephros region-derived endothelium. Blood **92:**908–919.
25. **Peng, J., L. Zhang, L. Drysdale, and G.-H. Fong.** 2000. The transcription factor EPAS-1/hypoxia-inducible factor 2α plays an important role in vascular remodeling. Proc. Natl. Acad. Sci. USA **97:**8386–8391.
26. **Rose, F., F. Grimminger, J. Appel, M. Heller, V. Pies, N. Weissmann, L. Fink, S. Schmidt, S. Krick, G. Camenish, M. Gassmann, W. Seeger, and J. Hanze.** 2002. Hypoxic pulmonary artery fibroblasts trigger proliferation of vascular smooth muscle cells: role of hypoxia-inducible transcription factors. FASEB J. **16:**1660–1661.
27. **Rosenberg, A. A., J. Kennaugh, S. L. Koppenhafer, M. Loomis, B. A. Chatfield, and S. H. Abman.** 1993. Elevated immunoreactive endothelin-1 levels in newborn infants with persistent pulmonary hypertension. J. Pediatr. **123:**109–114.
28. **Schiffrin, E. L.** 2005. Vascular endothelin in hypertension. Vasc. Pharmacol. **43:**19–29.
29. **Semenza, G. L.** 2004. O_2-regulated gene expression: transcriptional control of cardiorespiratory physiology by HIF-1. J. Appl. Physiol. **96:**1173–1177.
30. **Shimoda, L. A., D. J. Manalo, J. S. Sham, G. L. Semenza, and J. T. Sylvester.** 2001. Partial HIF-1 alpha deficiency impairs pulmonary arterial myocyte electrophysiological responses to hypoxia. Am. J. Physiol. Lung Cell. Mol. Physiol. **281:**L202–L208.
31. **Sugihara, C.** 2001. Treatment of persistent pulmonary hypertension of the newborn. J. Pediatr. **77:**S17–S24.
32. **Tanaka, Y., M. Nagai, T. Date, T. Okada, Y. Abe, S. Seki, M. Taniguchi, I. Taniguchi, and S. Mochizuki.** 2004. Effects of bradykinin on cardiovascular remodeling in renovascular hypertensive rats. Hypertens. Res. **27:**865–875.
33. **Tian, H., R. E. Hammer, A. M. Matsumoto, D. W. Russell, and S. L. McKnight.** 1998. The hypoxia-responsive transcription factor EPAS1 is essential for catecholamine homeostasis and protection against heart failure during embryonic development. Genes Dev. **12:**3320–3324.
34. **Wang, G. L., B.-H. Jiang, E. A. Rue, and G. L. Semenza.** 1995. Hypoxia-inducible factor 1 is a basic-helix-loop-helix-PAS heterodimer regulated by cellular O_2 tension. Proc. Natl. Acad. Sci. USA **92:**5510–5514.
35. **Wang, X., H. Osinska, G. W. Dorn II, M. Niemen, J. N. Lorenz, A. M. Gerdes, S. Witt, T. Kimball, J. Gulick, and J. Robbins.** 2001. Mouse model of desmin-related cardiomyopathy. Circulation **103:**2402–2407.
36. **Weinberger, B., K. Weiss, D. E. Heck, D. L. Laskin, and J. D. Laskin.** 2001. Pharmacologic therapy of persistent pulmonary hypertension of the newborn. Pharmacol. Ther. **89:**67–79.
37. **Wenger, R. H., and M. Gassman.** 1997. Oxygen(es) and the hypoxia-inducible factor-1. Biol. Chem. **378:**609–616.
38. **Zheng, X., J. L. Ruas, R. Cao, F. A. Salmons, Y. Cao, L. Poellinger, and T. Pereira.** 2006. Cell-type-specific regulation of degradation of hypoxia-inducible factor 1 alpha: role of subcellular compartmentalization. Mol. Cell. Biol. **26:**4628–4641.